American Mineralogist, Volume 99, pages 184–189, 2014

Crystal structures and stabilities of cristobalite-helium phases at high pressures

MASANORI MATSUI[1,*], TOMOKO SATO[2] AND NOBUMASA FUNAMORI[3]

[1]School of Science, University of Hyogo, Kouto, Kamigori, Hyogo 678-1297, Japan
[2]Department of Earth and Planetary Systems Science, Hiroshima University, Higashi-Hiroshima 739-8526, Japan
[3]Department of Earth and Planetary Science, University of Tokyo, Tokyo 113-0033, Japan

ABSTRACT

First-principles calculations were used to study the structural and energetic properties of cristobalite-He I and II at high pressures, both of which were recently found in high-pressure powder X-ray diffraction experiments of α-cristobalite with helium pressure-medium at room temperature. These calculations have revealed that both cristobalite-He I and II contain one helium atom per SiO_2 with the formula SiO_2He. It has also been revealed that cristobalite-He I is energetically favored above 6.4 GPa, cristobalite-He II is the stable phase at pressures between 1.7 and 6.4 GPa, and the mixture of cristobalite II and crystalline He is more stable than either cristobalite-He I or II below 1.7 GPa, in general agreement with the observation. Cristobalite-He I and II have been predicted to be monoclinic with space group $P2_1/c$, and rhombohedral with space group $R\bar{3}c$, respectively. The unit-cell parameters of both cristobalite-He I and II were re-determined from the previously measured high-pressure X-ray diffraction data on the basis of these predicted cells. There is an excellent agreement between the observed (re-determined) and calculated pressure dependence of the cell parameters for the both phases. The calculated X-ray diffraction patterns for both cristobalite-He I and II are also consistent with the observed data. Cristobalite-He I and II have been predicted to have molar volumes 21% larger at 10 GPa and 23% larger at 4 GPa than cristobalite II due to the penetration of helium atoms into large voids of the structure.

Keywords: Cristobalite-helium, high pressure, stability, first-principles calculations

INTRODUCTION

The structural and physical properties of silica (SiO_2) polymorphs and silica glass have been extensively studied, both experimentally and theoretically, because of their importance in the fields of geoscience, material science, and solid-state physics. Silica occurs in various crystal structures, including quartz, cristobalite, tridymite, coesite, and stishovite. Quartz and cristobalite show low-temperature (α) and high-temperature (β) modifications, and tridymite exists in many different crystalline forms. α-quartz is the stable phase at ambient conditions. Cristobalite and tridymite are high-temperature phases; coesite and stishovite are high-pressure phases; and α-cristobalite (hereafter simply cristobalite), tridymite, coesite, and stishovite all occur as metastable modifications at ambient conditions (Heaney 1994; Hemley et al. 1994).

Sato et al. (2011) and Shen et al. (2011) independently reported that a substantial amount of helium can dissolve into the large interstitial voids in silica glass at high pressures, greatly decreasing its compressibility. Synchrotron powder X-ray diffraction measurements using a diamond-anvil cell with helium pressure-medium under high pressures at room temperature allowed Sato et al. (2013) to find that cristobalite, which also includes large interstitial voids in its structure similar to silica glass, can also absorb a large amount of helium. They found that compression causes cristobalite (or cristobalite II) to transform to a new phase (cristobalite-He I) at about 8 GPa. Subsequent decompression caused the cristobalite-He I to transform to another new phase (cristobalite-He II) at about 7 GPa. They tentatively assigned cristobalite-He I to have orthorhombic symmetry and a molar volume about 30% greater than that of cristobalite; cristobalite-He II was assigned rhombohedral symmetry with a molar volume about 25% greater than that of cristobalite. However, the two phases' total helium uptakes and their crystal structures have yet to be reported. Here we use first-principles calculations to study the structural and energetic properties of both cristobalite-He I and II in detail.

CALCULATIONS

Calculations were performed with the Vienna Ab-initio Simulation Package (VASP) (Kresse and Furthmüller 1996) based on density functional theory. The projector augmented wave (PAW) method (Blöchl 1994; Kresse and Joubert 1999) was used in the generalized gradient approximation (GGA) for the exchange–correlation functional (Perdew et al. 1996) based on valence electron configurations of $3s^23p^2$, $2s^22p^4$, and $1s^2$ for Si, O, and He, respectively. We employed the GGA approach because it reproduces structural energy differences between silica polymorphs more accurately than does the local density approximation (LDA) (Demuth et al. 1999). The plane-wave cut-off energy was 700 eV, and k-point sampling was generally achieved using Monkhorst-Pack grids of 14 × 14 × 7, 6 × 6 × 4, 4 × 6 × 4, 4 × 6 × 4, and 8 × 8 × 8 for helium, cristobalite, cristobalite II, monoclinic cristobalite-He I or II, and rhombohedral cristobalite-

* E-mail: m.matsui@sci.u-hyogo.ac.jp

0003-004X/14/0001–184$05.00/DOI: http://dx.doi.org/10.2138/am.2014.4637

He II, respectively. Increasing the cut-off energy or the *k*-point grid produced essentially similar energies. A conjugate gradient or quasi-Newton algorithm was used to minimize the enthalpy of the system $H = U + PV$ by optimizing the cell parameters and the atomic coordinates at static conditions (0 K without zero-point vibrations) under crystal-symmetry constraints at a given pressure. Here, U is the internal energy, and P and V are the pressure and volume of the system of interest, respectively. The structure was optimized until the enthalpy converged to within 1×10^{-5} eV per unit cell.

RESULTS AND DISCUSSION

Cristobalite and cristobalite II

The reliability and applicability of the computations were assessed first by calculating the structures and energies of cristobalite and cristobalite II. The initial lattice parameters and atomic positions of Si and O were taken from observed data for cristobalite (Downs and Palmer 1994; Dera et al. 2011) and cristobalite II (Palmer and Finger 1994; Dove et al. 2000; Dera et al. 2011; the unit cells reported by Palmer and Finger and by Dove et al. were transformed to the $P2_1/c$ unit cells described by Dera et al.). Table 1 lists the observed and calculated cell parameters, and Si-O bond distances and Si-O-Si angles for cristobalite at 0.1 MPa and for cristobalite II at 3.5 GPa. For comparison, the table also lists the results of previous ab initio calculations using the GGA method for cristobalite (Demuth et al. 1999; Coe and Vanderbilt 2008). Figures 1 and 2 compare the observed and calculated cell parameters as a function of pressure for cristobalite and cristobalite II, respectively, and Figure 3 compares the volumes of both cristobalite and cristobalite II calculated at different pressures with observed values (Downs and Palmer 1994; Palmer and Finger 1994; Dove et al. 2000; Dera et al. 2011). The observed data for both cristobalite and cristobalite II were obtained at room temperature, while the present calculated

TABLE 1. Observed and calculated cell parameters, Si-O distances, and Si-O-Si angles in cristobalite at 0.1 MPa and in cristobalite II at 3.5 GPa

	Cristobalite at 0.1 MPa, space group $P4_12_12$			
	Obs[a]	Calc1[b]	Calc2[c]	Calc3[d]
a (Å)	4.9717(4)	5.073	5.119	5.073
c	6.9223(3)	7.080	7.168	7.085
V (Å^3)	171.10(1)	182.18	187.84	182.34
Si-O (Å)	1.603(1)	1.625	1.614	1.647
Si-O′	1.603(1)	1.624	1.614	1.645
Si-O-Si (°)	146.49(6)	148.46	154.22	144.5

	Cristobalite II at 3.5 GPa, space group $P2_1/c$				
	Obs[a]	Calc1[b]		Obs[a]	Calc1[b]
a (Å)	8.082(2)	8.255	Si2-O1 (Å)	1.594(1)	1.623
b	4.602(1)	4.709	Si2-O2	1.594(1)	1.623
c	9.058(2)	9.303	Si2-O4	1.598(3)	1.629
β (°)	121.82(1)	122.43	Si2-O4′	1.595(1)	1.624
V (Å^3)	286.26(6)	305.26	Si1-O1-Si2 (°)	139.3(4)	138.52
Si1-O1 (Å)	1.598(3)	1.625	Si1-O2-Si2	147.0(3)	146.31
Si1-O2	1.597(2)	1.615	Si1-O3-Si1	134.8(3)	134.65
Si1-O3	1.598(3)	1.629	Si2-O4-Si2	128.5(3)	131.71
Si1-O3′	1.597(2)	1.628			

[a] Observed values are from Downs and Palmer (1994) for cristobalite at 0.1 MPa, and from Dove et al. (2000) for cristobalite II at 3.5 GPa. For cristobalite II, the unit cells reported by Dove et al. (2000) are transformed as: **a**′ = –**a** – **c**, **b**′ = –**b**, and **c**′ = **c**.
[b] Present calculations.
[c] From Demuth et al. (1999).
[d] From Coh and Vanderbilt (2008).

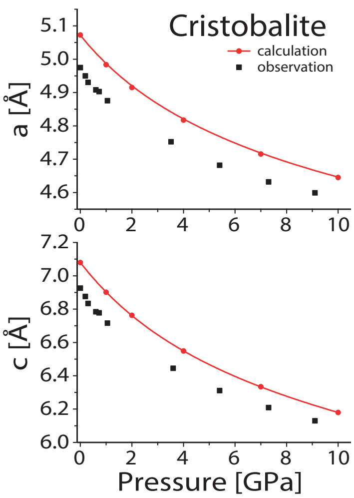

FIGURE 1. Pressure dependence of the observed (Downs and Palmer 1994; Dera et al. 2011) and calculated cell parameters of α-cristobalite. (Color online.)

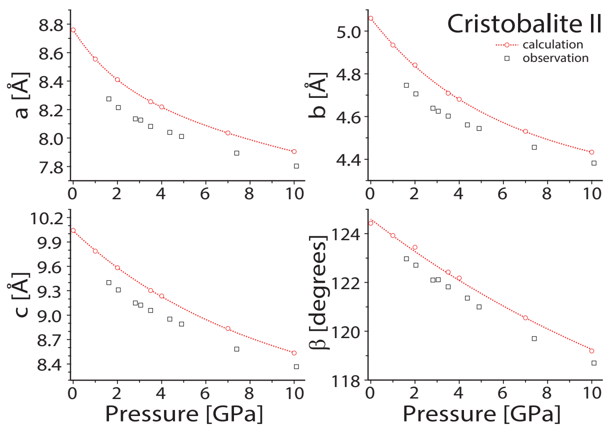

FIGURE 2. Pressure dependence of the observed (Palmer and Finger 1994; Dove et al. 2000; Dera et al. 2011) and calculated cell parameters of cristobalite II. (Color online.)

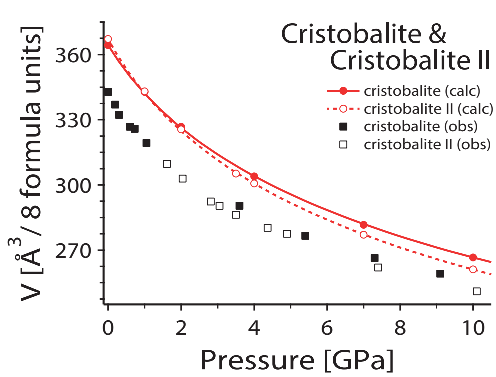

FIGURE 3. Observed and calculated pressure-volume equations of state of α-cristobalite and cristobalite II. Observed data are from Downs and Palmer (1994) and Dera et al. (2011) for α-cristobalite, and from Palmer and Finger (1994), Dove et al. (2000), and Dera et al. (2011) for cristobalite II. (Color online.)

values, as well as the data predicted previously for cristobalite, were derived at 0 K without zero-point vibrations.

The calculated structures of the two polymorphs are in good agreement with observation. At pressures up to about 10 GPa, the present calculations systematically overestimate the two phases' observed cell lengths and volumes by 2–3% and 4–7%, respectively (Table 1 and Figs. 1–3). Similarly, the previous calculations overestimate the cell parameters of cristobalite by 2–4% (Table 1). Such overestimation is typical of the GGA calculations of the exchange-correlation functionals used in both the present study and the previous calculations. At up to 10 GPa, the present calculated β angle in cristobalite II is overestimated by <0.5% (Fig. 2). Cristobalite II is calculated to have larger volumes than cristobalite at pressures below about 1 GPa; however, its volume relative to cristobalite becomes increasingly smaller with increasing pressure, consistent with the observed general trend (Fig. 3). The equation of state (EOS) parameters for cristobalite, obtained using the calculated P–V data and the third-order Birch-Murnaghan equation, are $K_0 = 13.27(24)$ GPa and $K_0' = 5.66(15)$, with V_0 fixed at 182.18 Å^3. These values are comparable to the values $K_0 = 11.0(4)$ GPa and $K_0' = 8.4(5)$, with V_0 fixed at 171.42 Å^3, observed by Dera et al. (2011). The similarly obtained EOS parameters for cristobalite II are $K_0 = 11.71(20)$ GPa and $K_0' = 5.36(12)$, with V_0 fixed at 367.20 Å^3. The calculated Si-O distances for each structure compare well with experimental results, although they are systematically 0.02–0.03 Å longer than the observed values (Table 1). This reflects the general tendency of GGA calculations to underbind the atoms, as described above. The differences in Si-O-Si angles between the observed and present calculated values are 1.3% for cristobalite at 0 GPa and less than 2.2% for cristobalite II at 3.5 GPa (Table 1).

The present calculations show that cristobalite is stable relative to cristobalite II by only 0.003 eV per formula unit at 0 GPa, while it is less stable above 2 GPa. This is in good agreement with the observation that cristobalite transforms to cristobalite II at about 1.5 GPa at room temperature (Palmer and Finger 1994; Dove et al. 2000).

Helium

Driessen et al. (1986) developed an EOS of helium at 0 K, based on their own isochoric measurements at pressures between 0.01 and 0.2 GPa and at temperatures from $T = 2$ K up to the liquid phase, along with other reported measured and theoretical data, including the measured isothermal compression data between 0.2 and 2 GPa at 4.2 K recorded by Stewart (1963). Using single-crystal X-ray diffraction measurements of solid helium from 1 to 58 GPa over the temperature range 46–400 K, Loubeyre et al. (1993) confirmed that their reduced EOS data to $T = 0$ K compare well with the EOS reported by Driessen et al. (1986). Our calculated EOS reproduces these data accurately over a wide pressure range to over 40 GPa (Fig. 4). The calculated c/a ratios are between 1.631 and 1.632 over the pressure range 0–40 GPa, close to the ideal value of 1.633, which is again consistent with the measured values of 1.630 ± 0.005 at high pressures up to 58 GPa reported by Loubeyre et al. (1993).

Cristobalite with helium

Cristobalite-He I was observed upon compression above 8.9 GPa, cristobalite-He II was observed between 6.1 and 4.1 GPa during subsequent decompression, and both cristobalite-He I and II were unquenchable to ambient pressure (Sato et al. 2013). Since cristobalite transforms to cristobalite II at about 1.5 GPa at room temperature without helium (Palmer and Finger 1994; Dove et al. 2000), we considered He atoms in cristobalite-He situated in the large voids of cristobalite II. The asymmetric unit of cristobalite II with space group $P2_1/c$ contains two independent Si and four independent O atoms, all at general positions. The initial lattice parameters and the initial atomic positions for both Si and O were taken from cristobalite II (Dove et al. 2000; Dera et al. 2011). In this study, two different He atoms were situated arbitrarily at general positions in the asymmetric unit of the cristobalite II lattice; thus, the unit cell contained 8 Si, 16 O, and 8 He atoms ($Z = 8$) with the formula SiO_2He. We tested several structural models with different initial He positions, and obtained two enthalpy-minimized structural models: model H for cristobalite-He I and model L for cristobalite-He II. Both models yielded lower enthalpies at high pressures than those for an equimolar mixture of cristobalite II (SiO_2) and crystalline He.

Figure 5 shows the two models' enthalpy differences, calculated for pressures up to 20 GPa, relative to the mixture of cristobalite II and crystalline He. Below 1.7 GPa, the mixture of cristobalite II and crystalline He is calculated to be more stable than either model L or H; however, model L is predicted to be the

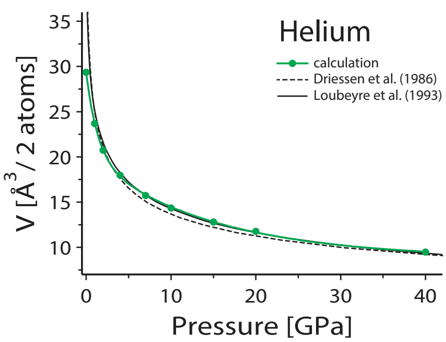

FIGURE 4. Calculated pressure-volume equation of state of crystalline helium, compared to the previous estimates by Driessen et al. (1986) and by Loubeyre et al. (1993). (Color online.)

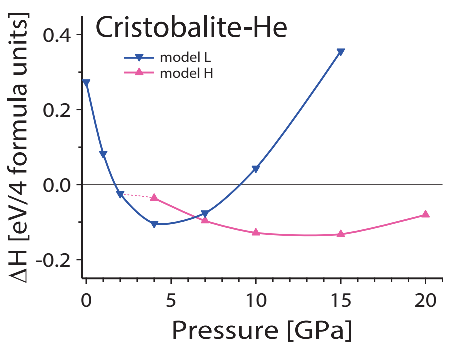

FIGURE 5. Calculated enthalpy differences of cristobalite-He I (model H) and II (model L) relative to an equimolar mixture of cristobalite II and crystalline helium, as a function of pressure up to 20 GPa. The dotted line shows the predicted phase transformation during decompression from model H at 4 GPa to model L at 2 GPa. (Color online.)

stable phase at pressures between 1.7 and 6.4 GPa, and model H is energetically most favored above 6.4 GPa. Model H existed metastably below 6.4 GPa but transformed to model L during decompression from 4 to 2 GPa, while model L remained metastable above 6.4 GPa. These predicted energetic properties at high pressures for both models are in agreement with the observed sequence of phase transitions in cristobalite (or cristobalite II) under compression with helium by Sato et al. (2013).

The model L structure, which has space group $P2_1/c$, can be converted into a rhombohedral structure with space group $R\bar{3}c$ within calculation errors for both the structures and energies between 0 and 15 GPa; the $R\bar{3}c$ structure for the model L gave the same structure with the $P2_1/c$. The $R\bar{3}c$ cell has half the volume of the $P2_1/c$ cell; it contains 4 SiO_2He per unit cell. The former structure relates to the latter through the cell transformation: $\mathbf{a}_r = \mathbf{a}_m$, $\mathbf{b}_r = (\mathbf{a}_m - \mathbf{b}_m - \mathbf{c}_m)/2$, and $\mathbf{c}_r = (\mathbf{a}_m + \mathbf{b}_m - \mathbf{c}_m)/2$, where the suffixes r and m represent the rhombohedral $R\bar{3}c$ and monoclinic $P2_1/c$ lattices, respectively.

Table 2 lists the computed cell parameters, fractional atomic coordinates, and bond distances and angles of the model H with the $P2_1/c$ lattice at 10 GPa, and also those of the model L with the $R\bar{3}c$ lattice at 4 GPa. The calculated cell parameters for model L based on the $P2_1/c$ lattice are also listed for comparison. The $R\bar{3}c$ cell parameters for model L at 4 GPa are converted to the $P2_1/c$ lattice as: a = 9.080 Å, b = 4.977 Å, c = 10.355 Å, β = 127.84°, which agree very closely with the values calculated (a = 9.078 Å, b = 4.976 Å, c = 10.363 Å, β = 127.82°) directly based on the $P2_1/c$ lattice (Table 2). The shortest distance between the O and He atoms is 2.741 Å in cristobalite-He II at 4 GPa, and 2.397 Å in cristobalite-He I at 10 GPa (Table 2). The minimum distance between two He atoms is 2.919 Å in cristobalite-He II at 4 GPa, and 2.107 Å in cristobalite-He I at 10 GPa. For reference, we note that the shortest He···He distance predicted for crystalline helium in this study is 2.334 Å at 4 GPa and 2.165 Å at 10 GPa.

Sato et al. (2013) measured the X-ray powder diffraction patterns of cristobalite-He I between 8.0 and 19.1 GPa, and of cristobalite-He II between 2.7 and 6.1 GPa. Their data are re-indexed here on the basis of monoclinic ($P2_1/c$) and rhombohedral ($R\bar{3}c$) unit cells for cristobalite-He I and II, respectively. Both structures were successfully indexed at each pressure, yielding the unit-cell parameters listed in Table 3. To facilitate the comparison of the two structures, we analyzed the diffraction pattern of cristobalite-He II measured by Sato et al. (2013) also using the $P2_1/c$ lattice. At each pressure between 2.7 and 6.1 GPa listed in Table 3, we found that the observed cell parameters of cristobalite-He II, determined based on the $P2_1/c$ lattice, agree with those based on the $R\bar{3}c$ lattice within the mutual errors, after the cell transformation described above.

The observed and calculated cell parameters of cristobalite-He I (model H) and II (model L), which are both based on the $P2_1/c$ lattice for better comparison, are compared in Figure 6. Figure 7 shows the observed and calculated pressure-volume EOSs of both cristobalite-He I and II. The EOS calculated here for cristobalite II (see Fig. 3) is also included for comparison. The figures show excellent agreement between the observed and computed pressure dependence of the lattice parameters and volumes for both cristobalite-He I and II. There is systematic slight overestimation of the computed cell lengths and volumes for both models H and L relative to the observed values; this is due to the established nature of the GGA calculations. The observed and calculated β angles are in excellent agreement for both cristobalite-He I and II (Fig. 6).

Table 2. Calculated structures of cristobalite-He I at 10 GPa, and of cristobalite-He II at 4 GPa

(a) Cristobalite-He I at 10 GPa, model H, space group $P2_1/c$, cell parameters: a = 8.062, b = 4.797, c = 9.491 Å, β = 120.43°, V = 316.47 Å^3			
Fractional coordinates:	x	y	z
Si1	0.6234	0.3883	0.8382
Si2	0.8726	0.1215	0.7119
O1	0.8001	0.2641	0.8249
O2	0.6910	0.4121	0.0293
O3	0.4354	0.1912	0.7477
O4	0.0373	0.3184	0.7146
He1	0.6328	0.5935	0.5320
He2	0.1379	0.3315	0.5136
	Bond distances (Å) and angles (°)		
Si1-O1	1.607	Si2-O1	1.611
Si1-O2	1.612	Si2-O2	1.613
Si1-O3	1.615	Si2-O4	1.619
Si1-O3′	1.616	Si2-O4′	1.617
shortest He-He	2.107	shortest He-O	2.397
Si1-O1-Si2	147.65	Si1-O2-Si2	143.84
Si1-O3-Si1	138.70	Si2-O4-Si2	135.81
(b) Cristobalite-He II at 4 GPa, model L, space group $R\bar{3}c$, cell parameters: a = 9.080 Å, α = 31.809°, V = 184.77 Å^3 (2V = 369.54 Å^3)			
Fractional coordinates:	x	y	z
Si	0.5622	x	x
O1	0.5	0.5	0.5
O2	0.8523	0.5 – x	0.25
He	0.8234	x	x
	Bond distances (Å) and angles (°)		
Si-O1	1.608	Si-O2 (×3)	1.619
shortest He-He	2.919	shortest He-O	2.741
Si-O1-Si	180.0	Si-O2-Si	143.34

Note: Cristobalite-He II at 4 GPa, model L, space group $P2_1/c$, cell parameters: a = 9.078, b = 4.976, c = 10.363 Å, β = 127.82 °, V = 369.78 Å^3.

Table 3. Pressure dependence of the observed lattice parameters of cristobalite-He I and II

Run no.[a]	P (GPa)	a (Å)	b	c	α or β (°)	V (Å^3)
Cristobalite-He I, space group $P2_1/c$, on compression						
3	8.9	8.027(8)	4.761(2)	9.544(18)	120.85(7)	313.1(5)
1	9.6	7.985(5)	4.745(1)	9.488(8)	120.63(5)	309.3(3)
3	10.4	7.942(3)	4.728(1)	9.420(5)	120.34(3)	305.3(2)
3	11.2	7.897(11)	4.705(3)	9.374(16)	120.29(10)	300.8(6)
3	12.0	7.880(2)	4.707(1)	9.344(4)	120.03(2)	300.0(1)
2	12.4	7.865(2)	4.702(0)	9.312(2)	119.86(2)	298.6(1)
1	12.7	7.851(4)	4.684(1)	9.281(6)	119.69(4)	296.5(2)
2	14.5	7.778(2)	4.648(0)	9.170(3)	119.28(2)	289.2(1)
1	15.7	7.755(5)	4.642(1)	9.141(7)	119.01(4)	287.7(3)
1	19.1	7.632(22)	4.628(6)	9.003(33)	118.26(21)	280.1(12)
Cristobalite-He I, space group $P2_1/c$, on decompression						
2	12.5	7.866(6)	4.693(1)	9.320(8)	120.06(5)	297.8(3)
2	10.7	7.950(9)	4.722(2)	9.414(13)	120.37(8)	304.9(5)
2	9.5	7.996(1)	4.753(0)	9.486(2)	120.62(1)	310.2(1)
3	8.4	8.072(0)	4.779(0)	9.584(0)	121.00(0)	316.9(0)
2	8.0	8.090(4)	4.793(1)	9.618(6)	121.20(4)	319.0(2)
Cristobalite-He II, space group $R\bar{3}c$, on decompression						
2	6.1	8.943(42)			31.36(15)	171.9(9)
3	4.8	8.971(31)			31.67(11)	176.7(6)
3	4.6	8.971(9)			31.69(3)	176.9(2)
2	4.1	8.975(49)			31.85(18)	178.8(10)
3	3.2	8.987(8)			32.25(3)	183.7(2)
3	2.7	8.988(9)			32.37(4)	185.0(2)

[a] See Sato et al. (2013) for details of the original X-ray diffraction data.

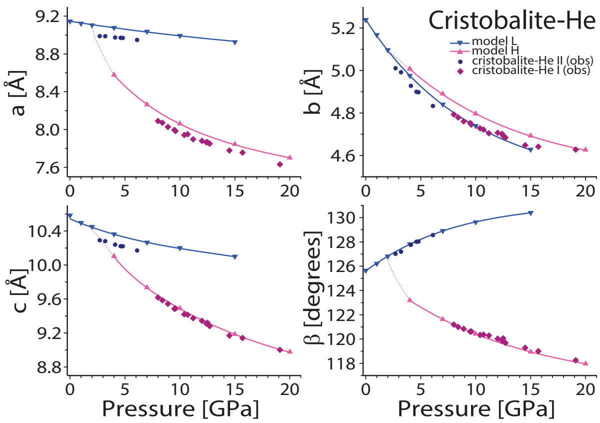

FIGURE 6. Calculated unit-cell parameters of cristobalite-He I (model H) and II (model L) as a function of pressure, together with observed data (Sato et al. 2013) re-determined in this study for comparison. The cell parameters of cristobalite-He II are plotted here based on the $P2_1/c$ lattice, instead of the final $R\overline{3}c$ lattice given in Table 3, for better comparison between the cristobalite-He I and II structures (see text). The dotted lines are the same as in Figure 5. (Color online.)

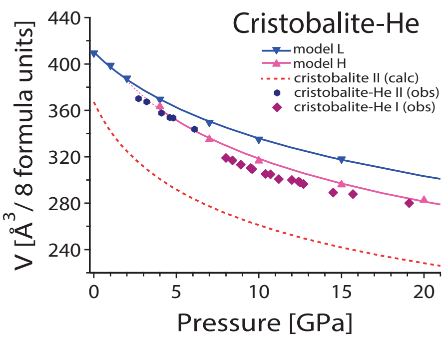

FIGURE 7. Observed (Sato et al. 2013) and calculated pressure-volume equations of state of cristobalite-He I (model H) and cristobalite-He II (model L). The calculated equation of state of cristobalite II is also shown for comparison. The dotted line is the same as in Figure 5. (Color online.)

Figure 8 compares the observed and calculated powder X-ray diffraction patterns of cristobalite-He I at 10.4 GPa and cristobalite-He II at 4.1 GPa. Since the calculated lattice parameters of the two phases reproduced the observed data very accurately over a wide pressure range (Figs. 6 and 7), we calculated the diffraction pattern for cristobalite-He I using the lattice parameters observed at 10.4 GPa (Table 3) and the atomic coordinates computed at 10 GPa (Table 2). The pattern for cristobalite-He II was calculated using the lattice parameters observed at 4.1 GPa (Table 3) and the atomic coordinates calculated at 4 GPa (Table 2) with space group $R\overline{3}c$. The observed diffraction patterns at 10.4 and 4.1 GPa compare very well with the calculated patterns for the mixture of the model H and cristobalite II, and for the mixture of the model L and cristobalite II (and possibly quartz), respectively. This confirms the validity of the present structural models H and L for cristobalite-He I and II, respectively.

As pressure decreases from 20 GPa, the calculated cell parameters (and all the independent atomic positions as well) of model

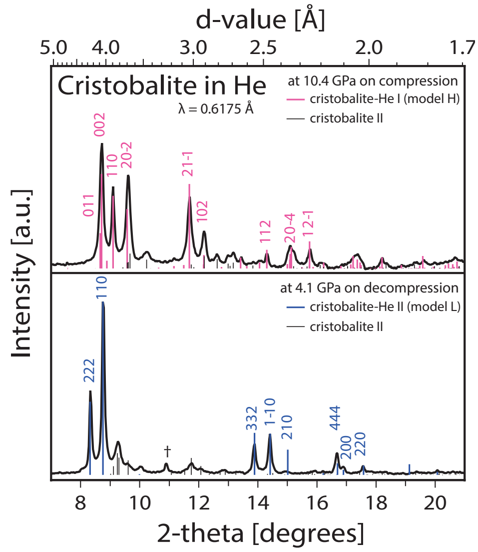

FIGURE 8. Comparison of observed and calculated X-ray diffraction patterns of cristobalite-He I (model H) and cristobalite-He II (model L). Peak intensities and positions were calculated assuming the space groups and atomic coordinates listed in Table 2 and the lattice parameters shown in Table 3. The peak intensities and positions of cristobalite II were calculated based on the data (the space group, atomic coordinates, and lattice parameters) listed in Dera et al. (2011). The molar ratio of cristobalite II to cristobalite-He I or II was fixed at 1/4. The dagger indicates a peak from quartz, which was present in the starting material (Sato et al. 2013). (Color online.)

H all approach, and finally agree with, those of model L within calculation errors at 2 GPa (Fig. 6). This shows a displacive-type phase transition from cristobalite-He I to II. The transition is an irreversible process, and once model L was formed at 2 GPa from model H, it was preserved metastably even after the pressure was increased above 6.4 GPa (also see Fig. 5).

Both cristobalite-He I and II show substantially larger volumes than cristobalite II (Fig. 7). Cristobalite-He I (model H) had a calculated volume of 316.47 Å^3 at 10 GPa, while that of cristobalite-He II (model L) was 369.54 Å^3 (per two unit cells for the $R\overline{3}c$ lattice) at 4 GPa (Table 2). These values are, respectively, 21 and 23% larger than the volumes of cristobalite II at the two pressures (260.99 and 300.69 Å^3, respectively) obtained from the EOS parameters of cristobalite II determined in this study; V_0 = 367.20 Å^3, K_0 = 11.71(20) GPa, and K_0' = 5.36(12). Similar substantial volume increases have been found in silica glass (Sato et al. 2011; Shen et al. 2011) and in melanophlogite (Yagi et al. 2007), a SiO_2 clathrate with large cages, due to the penetration of helium atoms into large interstitial voids in the structure upon compression with a helium pressure-medium.

The two models H and L of formula SiO_2He, respectively, reproduce very accurately the available observed energetic and structural high-pressure properties of cristobalite-He I and II. However, we also tried to find whether other structural models with different amounts of helium are possible for either cristobalite-He I or II. Using similar computational techniques as described above, we calculated several structures of formula Si_2O_4He, instead of SiO_2He, with different initial He positions in the cristobalite II lattice. However, no energetically favored configurations emerged at any pressure up to 20 GPa.

Sato et al. (2013) assigned cristobalite-He I and II as orthorhombic and rhombohedral, respectively. The previously proposed structure for cristobalite-He I should be revised according to the present results listed in Table 2. The rhombohedral lattice, reported for cristobalite-He II by Sato et al. (2013), with the cell parameters $a = 7.107(1)$ Å, $\alpha = 87.78(2)°$, and $Z = 8$ at 4.1 GPa, gives the same molar volume as the present work; however, it should also be replaced by the parameters listed in Table 2.

Finally, cristobalite-He II, with the $R\overline{3}c$ setting at 4 GPa given in Table 2, is computed to converge with decreasing pressure toward the "ideal" cubic high-cristobalite (β-cristobalite) structure with space group $Fd3m$ (Wyckoff 1925). Its calculated cell parameters and atomic coordinates at 0 GPa are $a = 9.147$ Å, $\alpha = 33.238°$, x(Si) = 0.5625, x(O2) = 0.7927, x(He) = 0.8155. The $R\overline{3}c$ structure is related to the $Fd3m$ structure through the cell transformation: $\mathbf{a}_r = \mathbf{a}_c + \mathbf{b}_c/2 + \mathbf{c}_c/2$, $\mathbf{b}_r = \mathbf{a}_c/2 + \mathbf{b}_c + \mathbf{c}_c/2$, and $\mathbf{c}_r = \mathbf{a}_c/2 + \mathbf{b}_c/2 + \mathbf{c}_c$, where the suffixes r and c represent the rhombohedral and cubic lattices, respectively. The $Fd3m$ structure is established in the limit $\cos\alpha \rightarrow 5/6$ ($\alpha \rightarrow 33.5573°$), x(Si) $\rightarrow$ 0.5625 (= 9/16), x(O2) $\rightarrow$ 0.75, and x(He) $\rightarrow$ 0.8125 (= 13/16) (compare the parameters at 0 GPa above with those at 4 GPa listed in Table 2). β-cristobalite is observed to be stable above 1743 K at 0 GPa, and it is considered to have a disordered structure (see Heaney 1994; and references therein); however, the structure of cristobalite-He II with the formula SiO_2He is ordered with the structural parameters at 4 GPa listed in Table 2. This is due to the existence of helium atoms in the large voids in the $R\overline{3}c$ structure. However, the present calculations were performed at 0 K without zero-point vibrations. Since the interactions between the SiO_2 framework and helium are very weak, a much greater mobility of the helium atoms is expected at finite temperatures.

Acknowledgments

The authors thank Artem Oganov, an anonymous reviewer, and Sergio Speziale (Associate Editor) for their constructive comments and helpful suggestions. This work was supported in part by JSPS KAKENHI Grant Number 24540520 to M.M., 25800295 to T.S., and 23654156, 25610130, 25287111 to N.F.

References cited

Blöchl, P.E. (1994) Projector augmented-wave method. Physical Review B, 50, 17953–17979.

Coe, S., and Vanderbilt, D. (2008) Structural stability and lattice dynamics of SiO_2 cristobalite. Physical Review B, 78, 054117.

Demuth, T., Jeanvoine, Y., Hafner, J., and Ángyán, J.G. (1999) Polymorphism in silica studied in the local density and generalized-gradient approximations. Journal of Physics: Condensed Matter, 11, 3833–3874.

Dera, P., Lazarz, J.D., Prakapenka, V.B., Barkley, M., and Downs, R.T. (2011) New insights into the high-pressure polymorphism of SiO_2 cristobalite. Physics and Chemistry of Minerals, 38, 517–529. *(In Table 5, the x parameter of O1 at 10.1 GPa, 823, should be replaced by 8230.)*

Dove, M.T., Craig, M.S., Keen, D.A., Marshall, W.G., Redfern, S.A.T., Trachenko, K.O., and Tucker, M.G. (2000) Crystal structure of the high-pressure monoclinic phase-II of cristobalite, SiO_2. Mineralogical Magazine, 64, 569–576.

Downs, R.T., and Palmer, D.C. (1994) The pressure behavior of α cristobalite. American Mineralogist, 79, 9–14.

Driessen, A., van der Poll, E., and Silvera, I.F. (1986) Equation of state of solid ^{4}He. Physical Review B, 33, 3269–3288.

Heaney, P.J. (1994) Structure and chemistry of the low-pressure silica polymorphs. In P.J. Heaney, C.T. Prewitt, and G.V. Gibbs, Eds., Silica: Physical Behavior, Geochemistry and Materials Application, vol. 29, p. 1–40. Reviews in Mineralogy, Mineralogical Society of America, Chantilly, Virginia.

Hemley, R.J., Prewitt, C.T., and Kingma, K.J. (1994) High-pressure behavior of silica. In P.J. Heaney, C.T. Prewitt, and G.V. Gibbs, Eds., Silica: Physical Behavior, Geochemistry and Materials Application, vol. 29, p. 41–81. Reviews in Mineralogy, Mineralogical Society of America, Chantilly, Virginia.

Kresse, G., and Furthmüller, J. (1996) Efficient iterative schemes for *ab initio* total-energy calculations using a plane wave basis set. Physical Review B, 54, 11169–11186.

Kresse, G., and Joubert, D. (1999) From ultrasoft pseudopotentials to the projector augmented-wave method. Physical Review B, 59, 1758–1775.

Loubeyre, P., LeToullec, R., Pinceaux, J.P., Mao, H.K., Hu, J., and Hemley, R.J. (1993) Equation of state and phase diagram of solid ^{4}He from single-crystal X-ray diffraction over a large P-T domain. Physical Review Letters, 71, 2272–2275.

Palmer, D.C., and Finger, L.W. (1994) Pressure-induced transition in cristobalite: An X-ray powder diffraction study to 4.4 GPa. American Mineralogist, 79, 1–8.

Perdew, J.P., Burke, K., and Ernzerhof, M. (1996) Generalized gradient approximation made simple. Physical Review Letters, 77, 3865–3868.

Sato, T., Funamori, N., and Yagi, T. (2011) Helium penetrates into silica glass and reduces its compressibility. Nature Communications, 2, 345.

Sato, T., Takada, H., Yagi, T., Gotou, H., Okada, T., Wakabayashi, D., and Funamori, N. (2013) Anomalous behavior of cristobalite in helium under high pressure. Physics and Chemistry of Minerals, 40, 3–10.

Shen, G., Mei, Q., Prakapenka, V.B., Lazor, P., Sinogeikin, S., Meng, Y., and Park, C. (2011) Effect of helium on structure and composition behavior of SiO_2 glass. Proceedings of the National Academy of Sciences, 108, 6004–6007.

Stewart, J.W. (1963) Compression of Solid He^3 and He^4 to 20000 bars. Physical Review, 129, 1950–1951.

Wyckoff, R.W.G. (1925) The crystal structure of the high temperature form of cristobalite (SiO_2). American Journal of Science, 9, 448–459.

Yagi, T., Iida, E., Hirai, H., Miyajima, N., Kikegawa, T., and Bunno, M. (2007) High-pressure behavior of SiO_2 clathrate observed by using various pressure media. Physical Review B, 75, 174115.

Manuscript received June 16, 2013
Manuscript accepted September 10, 2013
Manuscript handled by Sergio Speziale